Backscatter suppression via blind signal separation for a 532 nm underwater chaotic lidar rangefinder

David W. Illig[1], Luke K. Rumbaugh[1], Mahesh K. Banavar[1], Erik M. Bollt[2], William D. Jemison[1]
Department of [1]Electrical and Computer Engineering, [2]Mathematics
Clarkson University
Potsdam, NY
illigdw@clarkson.edu

Abstract— **Blind signal separation is applied to suppress backscatter for a 532 nm chaotic lidar underwater rangefinder. When operating in turbid waters, chaotic lidar returns contain information for both submerged objects and an optical backscatter "clutter" component. The statistical digital signal processing technique of blind signal separation (BSS) is applied to dynamically measure and cancel out the backscatter component before computing range to the desired object. Results from simulations and laboratory experiments are presented to demonstrate the combined chaotic/BSS approach. The chaotic/BSS approach extends operating range by almost 40% and achieves centimeter-order range accuracy. Receiver operating curves are simulated for the chaotic/BSS approach, which show convergence towards the ideal classifier in several conditions of interest.**

Keywords—underwater optical ranging, blind signal separation, chaotic lidar, clutter suppression

I. INTRODUCTION

Hybrid lidar-radar is used to perform underwater detection, ranging, and imaging for applications that require high resolution and accuracy over relatively short distances [1]. A radar-like intensity modulation is applied to laser light and transmitted through the underwater optical channel, where it is reflected by objects in the scene. The radar modulation envelope of the return signal is then recovered at the optical receiver and undergoes coherent radar detection and digital signal processing (DSP). Absorption and scattering are substantial challenges for underwater hybrid lidar-radar systems. Absorption can be reduced by using lasers in the blue-green portion of the visible spectrum [2].

Of particular concern in the ranging application is backscatter, which occurs when photons are scattered backwards and arrive at the detector without reaching the desired object. Backscattered light contains no information regarding the desired object, and it reduces range resolution and accuracy. In hybrid lidar-radar, the object return can be detected in the presence of backscatter by applying a modulation frequency above the backscatter cutoff frequency (about 100 MHz in turbid waters) [3]. A variety of waveforms have been investigated in previous work, including continuous wave [4],

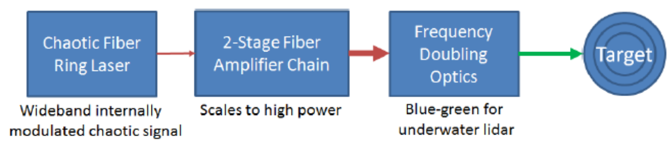

Figure 1. Chaotic lidar transmitter for underwater ranging

pulsed [5-6], stepped frequency sweep [7-8], linear frequency sweep [9], and chaotic waveforms [10]. Backscatter can be further suppressed by applying DSP algorithms to the lidar return signal. The statistical processing technique of blind signal separation (BSS) has shown the ability to separate the object and backscatter promising results for both stepped and linear frequency sweeps [11-12]. For each of these waveforms BSS was therefore able to suppress backscatter and extend operating range. We hypothesize that as chaotic lidar provides a similar form of lidar return, BSS should allow dynamic separation of the object and backscatter returns for chaotic lidar, thereby increasing ranging performance.

This paper demonstrates a chaotic/BSS approach which combines the advantages of chaotic lidar with the enhanced backscatter suppression provided by blind signal separation. Section II provides a brief overview of both chaotic lidar and blind signal separation. The experimental setup, simulation methodology, and processing procedure are presented in Section III. Simulated and experimental results are presented in Section IV. Finally, Section V summarizes this work and suggests areas for future investigation.

II. BACKGROUND

A. Chaotic Lidar

Chaotic lidar sensors provide high-resolution ranging, pulse compression gain, and near-optimal noise rejection via cross-correlating (matched filter) receivers. This work uses a custom 532 nm chaotic source to probe the channel with a wideband chaotic intensity modulation [10]. The chaotic signal is a noise-like signal with high pulse compression gain and narrow correlation peaks [13]. Figure 1 shows the basic blocks of the 532 nm chaotic lidar transmitter. The transmitter consists of three main components: an internally modulated chaotic ytterbium-doped fiber ring laser, two fiber amplifiers, and a second-harmonic generation (SHG) crystal used as an optical

978-0-933957-43-5 ©2015 MTS

frequency doubler. The 1064 nm fiber laser has a ring cavity whose length is extended to 120 m using passive fiber. This long cavity allows thousands of resonant modes to lase simultaneously, generating wide bandwidth modulation from DC up to multiple GHz [14]. This bandwidth supports centimeter-order range resolution, while the higher frequency content is desirable for backscatter suppression. Unambiguous range is equal to half the length of the fiber ring cavity.

The fiber ring laser's infrared output must be frequency doubled and amplified to counter absorption in the underwater environment. Two ytterbium-doped fiber amplifier (YDFA) stages boost the ring laser output while preserving the chaotic waveform. A periodically poled SHG crystal is used to convert the laser wavelength from 1064 nm infrared to 532 nm green. The chaotic modulation signal can then be transmitted through the underwater channel with significantly reduced absorption. The return signal received after probing the channel corresponds to a reflectivity profile of the water, containing both submerged objects and backscatter. The unwanted backscatter contribution can be suppressed through DSP so that the desired object can be detected.

B. Blind Signal Separation

Blind signal separation is a technique in which observations of several signals are separated into independent signal components based on an assumption of statistical independence [15-16]. The basic model assumes that an array of sensors, X, has observed a mixture of the unknown signals, S:

$$X = AS \tag{1}$$

where A is the so-called "mixing" matrix and depends on the individual sensors. The mixing matrix A is typically considered to be unknown, with the number of sources either being treated as an unknown or defined by the application. The number of rows in X matches the number of sensors, while the number of columns is equal to the number of observations. The number of rows in A corresponds to the number of sensors, while the number of columns is equal to the number of sources. Finally, the source matrix S has one row for each source and one column for each observation. The objectives of BSS is to invert the mixing operation so that the observations X may be transformed into an estimate of the sources S.

This work builds an array of observations from multiple snapshots of the underwater channel, modeling a single sensor deployed on a moving platform. This model reflects the design of several deployed and prototype underwater lidar systems, which typically utilize a single, high-sensitivity photodetector as the optical receiver [17]. The underwater optical channel is assumed to be homogeneous, therefore all measurements should contain the same contribution from backscatter. Relative motion between the sensor platform and object of interest will cause each observation to contain a different object return.

The physical reality of this application supports the assumption of independent sources: backscattered photons never reached the object of interest and therefore should be independent of the object return. In this work, the principal component analysis form of BSS is used to separate the object and backscatter returns. We assume that these are the only signal sources in the scene. Under the channel homogeneity assumption, the backscatter components in each snapshot are highly correlated and will occupy the first subspace after decomposition. The second subspace will contain the source with the next highest correlation energy, namely the object return. The observation matrix X can be decomposed as:

$$X = U\Sigma V^T = U \begin{bmatrix} s_{BSN} & 0 \\ 0 & s_{OBJ} \end{bmatrix} V^T \tag{2}$$

where U is a unitary matrix, the columns of V are the eigenvectors of the matrix X^TX, the diagonal elements of Σ are the square roots of the eigenvalues of X^TX, and s_{BSN} and s_{OBJ} are the singular values corresponding to the backscatter and object returns, respectively. By setting the element corresponding to s_{BSN} to zero, an estimate of the object signal source can be obtained. Removing the first subspace in this way should suppress backscatter, increasing the signal-to-interference ratio (SIR) such that a weak object return can be detected in scenarios with high backscatter. This should enable the combined chaotic/BSS approach to detect objects at extended ranges while maintaining high range resolution.

III. Methodology

A. Experimental Procedure

The experimental setup used in this work is shown in Figure 2, with selected experimental and simulation parameters listed in Table 1. The chaotically-modulated 532 nm laser beam is split into a reference copy which is collected by a high-speed photodetector (PD) (Alphalas UPD-200), and a probe signal that is directed into the underwater channel. A white target is mounted to a translation stage in a 2.2 m long water tank. The target is moved in 2.5 cm increments from an initial position of 0.2 m to a final position of 2.0 m. A photomultiplier tube (PMT) (Photonis 5-stage PMT) collects light reflected off the desired object as well as backscattered photons. The outputs of the detectors are amplified with 40 dB, 1 GHz bandwidth low noise amplifiers (Mini-Circuits ZKL-1R5) before being digitized by a high-speed oscilloscope (Agilent Infiniium 54845A). Premier Value® liquid antacid was used as a scattering agent in the experiments, with a Wetlabs™ C-Star transmissometer used to measure the beam attenuation coefficient.

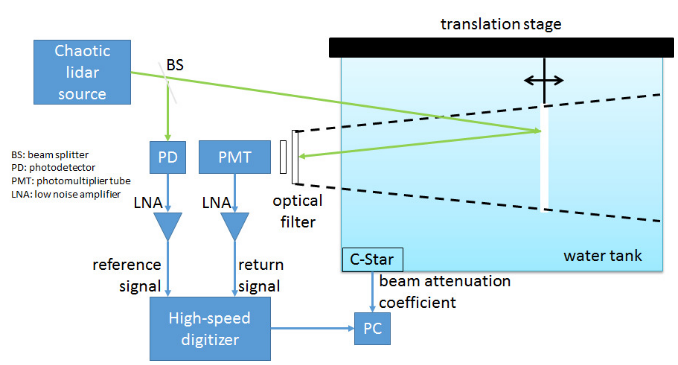

Figure 2. Experimental setup

Table 1. Experimental and simulation parameters

Parameter	Value	Unit
Source-receiver separation	10.0	cm
Receiver-object distance	0.2 – 2.0	m
Wavelength	532	nm
Optical power	50	mW
Receiver field-of-view	3.0	deg
Receiver bandwidth	1.5	GHz
Analog-digital converter bits	8	bits
Sampling rate	8	GSPS
Samples per snapshot	512	kS
Effective dwell time	64.8	μs
Beam attenuation coefficient	4.1	m^{-1}

Following digitization, the reference and return signals are transmitted to a PC, where they are cross-correlated. This results in an impulse response measurement of the scene. At this point, chaotic lidar detects the temporal shift between reference and return, resulting in an impulse response measurement of the scene from which range is calculated. A set of impulse responses from four subsequent snapshots are used to build the observation matrix for the chaotic/BSS approach. The observation matrix is decomposed as outlined in Eq. (2), with the backscatter component set to zero. Chaotic/BSS uses the shift of the resulting signal after backscatter is suppressed to compute range.

B. *Simulation Approach*

This work uses the Waveform Response 3D Model (WR3D) simulation tool to predict performance. WR3D is based on the method of moments and the solution of the radiative transfer equation in the small-angle diffusion approximation [18-20]. This tool allows full control of a variety of source, receiver, water, and geometry parameters, which are used to generate an impulse response matching actual experimental conditions. The simulation approach used in this work is summarized in Figure 3 and consists of three major steps. In the first step, WR3D is used to calculate the object and backscatter amplitude functions. In the second step, the impulse response computed by WR3D is convolved with a record of the transmitted chaotic waveform to simulate the chaotic lidar return detected at the PMT. Noise is optionally added at this point, with the simulated return signal cross-correlated with the reference to obtain the impulse response. BSS processing is applied in the third step, where the return signal is decomposed into two subspaces, representing the backscatter and target returns.

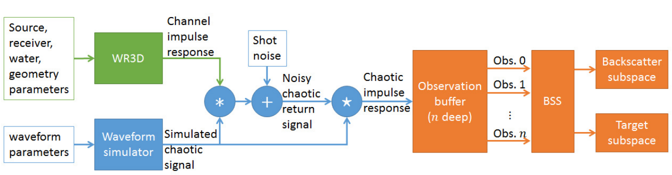

Figure 3. Block diagram showing simulation processing steps: 1. model underwater channel with WR3D (green); 2. model chaotic signal propagating through channel (blue); 3. apply BSS processing (orange).

IV. RESULTS

Results from simulations and experiments are presented. First, sample experimental impulse responses are shown with and without BSS. This is followed by simulated and experimental range results. Finally, simulated probability of detection curves are presented to show predicted performance of the chaotic/BSS approach as a function of signal-to-noise ratio (SNR).

A. *Demonstration of Chaotic/BSS Backscatter Suppression*

Example impulse responses are shown in Figure 4 and Figure 5 illustrating benefits of applying BSS to chaotic lidar. Figure 4 shows a case with a strong object return detectable by both chaotic lidar and chaotic/BSS, demonstrating that BSS can potentially enhance resolution: the full-width at half maximum (FWHM) of the object peak with chaotic lidar is about 22 cm, while chaotic/BSS reduces the FWHM to about 8.5 cm. Figure 5 shows a case with a weak object return in the rolloff from a strong backscatter return, a scenario in which detection would be difficult using chaotic lidar alone. In the chaotic/BSS approach, the backscatter and object returns appear in different components after applying PCA. This demonstrates that the object peak can be easily detected when the correct component is analyzed. In this example, the SIR increased from -7.7 dB to +8.4 dB by applying BSS – an improvement of 16.1 dB. These results demonstrate the potential for the chaotic/BSS approach to enhance ranging performance.

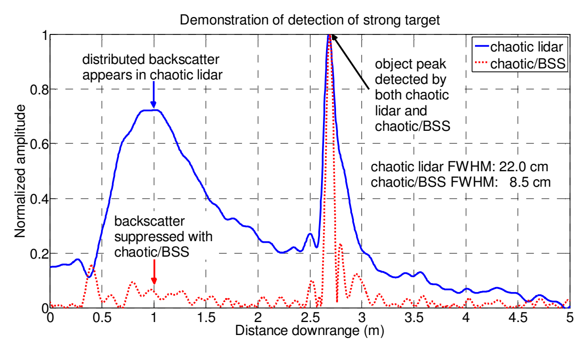

Figure 4. Demonstration of strong target scenario: chaotic lidar (blue) measures backscatter and desired object; chaotic/BSS (red) suppresses backscatter and reduces target peak width.

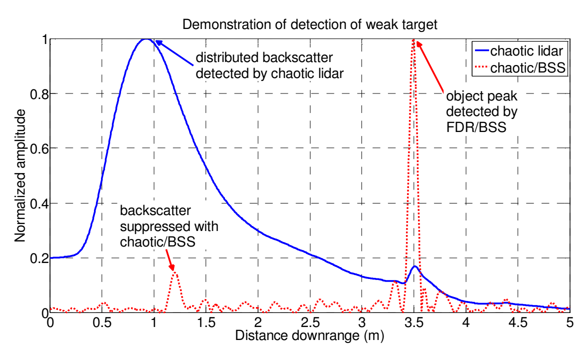

Figure 5. Demonstration of weak target scenario: chaotic lidar (blue) detects backscatter; chaotic/BSS (red) detects the object.

B. *Range Results*

Range results for both experiment and simulation are shown in Figure 6 and Figure 7, respectively. The turbidity in both cases was $c = 4.1\ \mathrm{m}^{-1}$, with the maximum test target position of 2.0 m downrange corresponding to 8.2 attenuation lengths (a.l.). Received power drops by roughly one-third for each attenuation length traveled. In both cases the chaotic/BSS technique is able to track the target for extended ranges compared to chaotic lidar alone. This is because in the chaotic lidar approach, the return is eventually dominated by backscatter, such that the range detected corresponds to the center of the volumetric backscatter distribution. In the experiments, chaotic lidar tracked the target to 1.26 m (5.17 a.l.), while in simulation chaotic lidar tracked the target to 1.50 m (6.15 a.l.). Once blind signal separation is applied, both the experiment and simulation can track the target to at least 2.0 m (8.2 a.l.). Note that the WR3D tool predicts extended performance for chaotic lidar that is not seen in experiment; this may potentially be caused by differences in target albedo and/or scattering coefficient.

Range error was also calculated for the experimental range measurements. The effects of noise and forward scatter are both visible in the experimental range error data shown in Figure 8. The oscillations in error are believed to be due to noise shifting the range measurement between adjacent correlation bins. Small-angle forward scattering causes path length increases on the return trip from the object, resulting in the increasing range error trends. For the chaotic lidar data, a best fit slope suggests an increase in range error of approximately 2.0 cm per meter

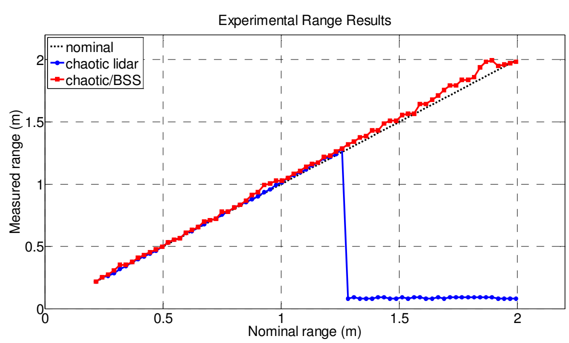

Figure 6. Experimental range results for chaotic lidar (blue) and chaotic/BSS (red) approaches

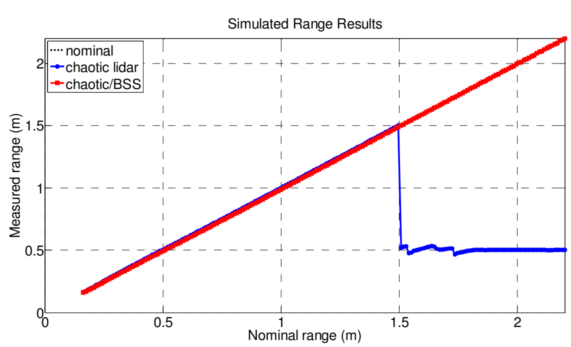

Figure 7. Simulated range results for chaotic lidar (blue) and chaotic/BSS (red) approaches

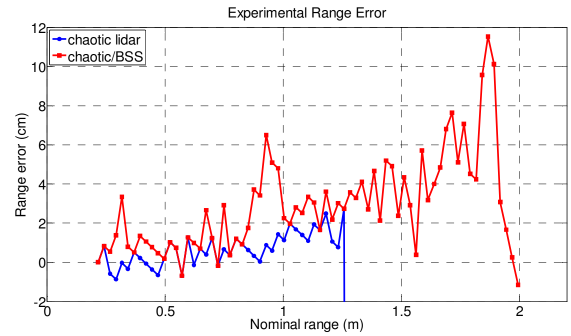

Figure 8. Experimental range error for chaotic lidar (blue) and chaotic/BSS (red) approaches

downrange, in the region where the test target could be detected. For chaotic/BSS, this slope increases slightly to 2.8 cm per meter downrange. These results show that while chaotic/BSS is not suppressing forward scatter, the mean range errors remain on the order of a few centimeters.

C. *Probability of Detection Simulations*

A series of simulations were performed to compute the receiver operating curves (ROC) for both chaotic lidar and chaotic/BSS. Each point on an ROC curve was generated by running 4000 simulations at a fixed set of conditions including Gaussian noise, analyzing the resulting impulse responses, and counting the number of false alarms and correct detections for a fixed detection threshold. Impulse response data were normalized into the range [0, 1] for this process. Each curve was generated by repeating this process while varying the amplitude detection threshold from 0 to 1 for a fixed signal-to-noise ratio (SNR). SNR levels of +10, 0, and -10 dB were used in the simulations. Signal-to-interference ratio (SIR) conditions corresponding to a strong target scenario (SIR=+10 dB), target and backscatter with equal amplitude (SIR=0 dB), and weak target scenario (SIR=-10 dB) were simulated as the various noise levels were applied to the data.

Figure 9 through Figure 11 show results for signal-to-noise ratios of +10, 0, and -10 dB for the strong target, equal amplitude, and weak target cases. In all scenarios, chaotic/BSS is always a better classifier than chaotic lidar alone. This is a result of the increased backscatter suppression: for a sufficiently high threshold, the object peak is the only peak to be detected in the chaotic/BSS approach (consider for example the impulse response shown in Figure 5 with a detection threshold above 0.2). For the high SNR case of Figure 9, chaotic/BSS converges towards the ideal classifier for all three SIR scenarios, while chaotic lidar converges to the random classifier as the target return becomes weaker relative to backscatter. As shown in Figure 10, lowering the SNR to 0 dB degrades the chaotic/BSS classifier for a weak target return, while the other classifiers are largely unchanged. When the SNR is reduced to -10 dB in Figure 11, the performance of the chaotic/BSS classifier seriously degrades as the target return becomes weaker. These results justify the additional processing of the chaotic/BSS approach for scenarios with poor SNR or weak target returns.

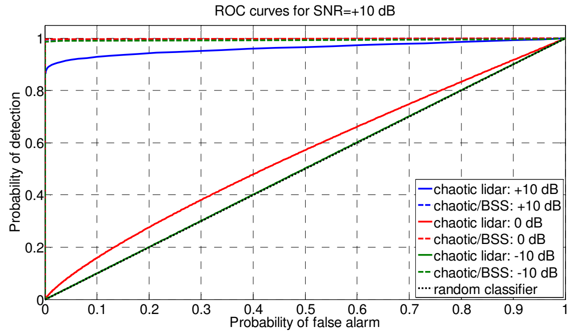

Figure 9. ROC curves for SNR=+10 dB for strong target (blue), equal amplitude (red), and weak target (green) cases.

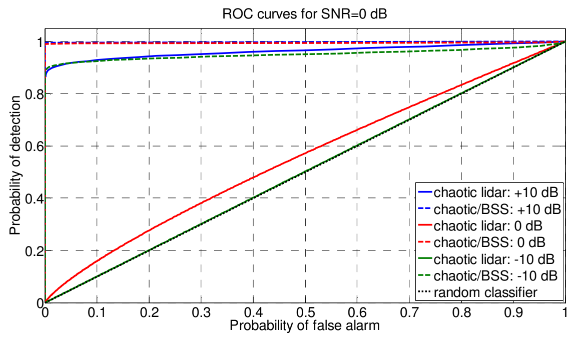

Figure 10. ROC curves for SNR=0 dB for strong target (blue), equal amplitude (red), and weak target (green) cases.

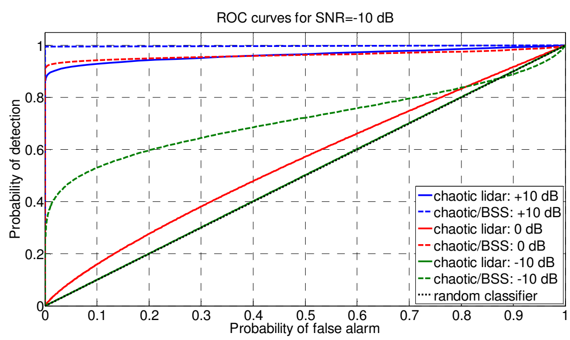

Figure 11. ROC curves for SNR=-10 dB for strong target (blue), equal amplitude (red), and weak target (green) cases.

V. SUMMARY

This work demonstrates the ability of blind signal separation to enhance a 532 nm underwater chaotic lidar rangefinder. The wide bandwidth of chaotic lidar allows for high-resolution ranging and some backscatter suppression, while unambiguous range can be increased simply by adding more fiber to the fiber ring laser. While the chaotic lidar measures backscatter and object returns simultaneously, blind signal separation was shown to be able to suppress the backscatter component. The combined chaotic/BSS approach was therefore able to increase effective signal-to-interference ratio, substantially improve detection performance over chaotic lidar alone, and extend range performance while maintaining centimeter-order accuracy. Target tracking was achieved to over 8 attenuation lengths with backscatter suppressed by approximately 15 dB.

Future work will aim to find the breakdown point of this approach, explore channel characterization applications, and consider the implications of the properties of the chaotic waveform on blind signal separation. While in the ranging application the goal of chaotic/BSS was to remove the backscatter return, the information contained in the backscatter subspace may be of value for characterization measurements including turbidity and scattering particle measurements for oceanography and channel identification and equalization for optical communications [21]. Future work should also aim to characterize the distributions of the backscatter and object return components obtained when using the chaotic lidar transmitter, as this will allow for a formalization of the chaotic/BSS approach.

ACKNOWLEDGMENT

This work was sponsored in part by the Office of Naval Research under grant numbers N000141010906 and N000141410358, and by the Department of Defense Science, Mathematics, and Research for Transformation (SMART) scholarship program. The authors thank Dr. Linda Mullen at NAVAIR for use of the WR3D tool and photomultiplier tube for these experiments. Any opinions, findings, and conclusions ore recommendations expressed in this material are those of the authors and do not necessarily reflect the views of the Office of Naval Research or the Department of Defense.

REFERENCES

[1] LJ Mullen and VM Contarino. “Hybrid Lidar-Radar: Seeing through the Scatter,” *IEEE Microwave Magazine*, 1(3):42-48 (2000).

[2] CD Mobley. *Light and Water*. San Diego: Elsevier Science (1994).

[3] F Pellen, X Intes, P Olivard, Y Guern, J Cariou, and J Lotrian. “Determination of sea-water cut-off frequency by backscattering transfer function measurement,” *J. Phys. D: Appl. Phys.* 33:349-354 (2000).

[4] A Laux, L Mullen, P Perez, and E Zege. “Underwater laser range finder,” *Proc. SPIE 8372 Ocean Sensing and Monitoring IV* (2012).

[5] B Cochenour, L Mullen, and J Muth. “Modulated pulse laser with pseudorandom coding capabilities for underwater ranging, detection, and imaging,” *Appl. Opt.*, 50(33):6168-6178 (2011).

[6] S O’Connor, LJ Mullen, and B Cochenour. “Underwater modulated pulse laser imaging system,” *Optical Engineering*, 53(5) (2014).

[7] DW Illig, WD Jemison, L Rumbaugh, R Lee, A Laux, and L Mullen. “Enhanced hybrid lidar-radar ranging technique,” *Proc. OCEANS 13 MTS/IEEE San Diego* (2013).

[8] DW Illig, WD Jemison, RW Lee, A Laux, LJ Mullen. “Optical Ranging Techniques in Turbid Waters,” *Proc. SPIE 9111 Ocean Sensing and Monitoring VI* (2014).

[9] DW Illig, A Laux, RW Lee, WD Jemison, and LJ Mullen. “FMCW optical ranging technique in turbid waters,” *Proc. SPIE 9459: Ocean Sensing and Monitoring VII* (2015).

[10] LK Rumbaugh, EM Bollt, WD Jemison, and Y Li. “A 532 nm Chaotic Lidar Transmitter for High Resolution Underwater Ranging and Imaging,” *Proc. OCEANS 13 MTS/IEEE San Diego* (2013).

[11] DW Illig, L Rumbaugh, WD Jemison, A Laux, and L Mullen. “Statistical backscatter suppression technique for a wideband hybrid lidar-radar ranging system,” *Proc. OCEANS 14 MTS/IEEE Newfoundland* (2014).

[12] DW Illig, LK Rumbaugh, MK Banavar, and WD Jemison. “Blind Signal Separation for Underwater Lidar Applications,” *Proc. 35th International Workshop on Bayesian Inference and Maximum Entropy Methods in Science and Engineering* (2015).

[13] FY Lin and JM Liu. “Chaotic Lidar,” *IEEE J. Sel. Topics Quantum Electron.*, 10(5):991-997 (2004).

[14] QL Williams, J Garcia-Ojalvo, and R Roy. “Fast intracavity polarization dynamics of an erbium-doped fiber ring laser: Inclusion of stochastic effects,” *Phys. Rev. A*, 55(3):2376-2386 (1997).

[15] GD Clifford. “Blind Source Separation: Principal & Independent Component Analysis,” in *MIT OpenCourseWare* (2007).

[16] A Hyvärinen and E Oja. “Independent Component Analysis: Algorithms and Applications,” *Neural Networks*, 13(4/5):411-430 (2000).

[17] JS Jaffe, KD Moore, J McLean, and MP Strand. “Underwater Optical Imaging: Status and Prospects,” *Oceanography*, 14(3):64-75 (2001).

[18] EP Zege, IL Katsev, and IL Polonsky. "Multicomponent approach to light propagation in clouds and mists," *Appl. Opt.* 32(15):2803-2812 (1993).

[19] EP Zege, AP Ivanov, and IL Katsev. *Image Transfer Through a Scattering Medium*. Heidelberg: Spinger-Verlag (1991).

[20] EP Zege, IL Katsev, AS Prikhach, GD Ludbrook, and P Bruscaglioni. "Analytical and computer modeling of the ocean lidar performance," *Proc. SPIE 5059: 12th International Workshop on Lidar Multiple Scattering Experiments* (2002).

[21] LK Rumbaugh, MK Banavar, and WD Jemison. “Underwater optical impulse response measurement using a chaotic lidar sensor,” *Proc. SPIE 9459: Ocean Sensing and Monitoring VII* (2015).